Rate-equation approach for frequency-modulation mode locking using the moment method

Nicholas G. Usechak and Govind P. Agrawal

The Institute of Optics, University of Rochester, Rochester, New York 14627, and Laboratory for Laser Energetics, University of Rochester, Rochester, New York 14623

Received March 30, 2005; accepted May 27, 2005

A semianalytic approach based on the moment method is used for investigating pulse evolution in mode-locked lasers in which intracavity dispersive and nonlinear effects play a significant role. Its application to an FM mode-locked laser allows us to perform fast parametric studies while predicting the important pulse parameters. When third-order dispersive effects are negligible, a fully analytic treatment is developed that predicts how cavity parameters affect the final steady state. Our analytic approach also allows us to predict relaxation-oscillation behavior as the pulse approaches its steady state. We use this technique to investigate novel aspects specific to FM mode-locked lasers such as stability of and switching between the multiple steady-state solutions. All results obtained are in excellent agreement with numerical simulations. © 2005 Optical Society of America

OCIS codes: 140.3430, 140.4050, 140.3510.

1. INTRODUCTION

Since closed-form solutions do not exist for the pulses produced by most mode-locked lasers, numerical simulations are essential and therefore frequently used. However, numerical investigations can require substantial computation time, especially in the presence of dispersive and nonlinear effects. In view of this limitation, parametric studies are not convenient in assisting experimentalists in the optimization of mode-locked lasers. In our study, we seek to overcome this limitation by using the moment method[1] in conjunction with the master equation governing the mode-locking phenomenon. This approach reduces the underlying partial differential equation into a few coupled algebraic equations. Since these equations can be solved rapidly, they allow parametric studies to be performed without the issues relating to computation time or complexity that plague rigorous numerical simulations. This technique should be attractive to experimentalists working in the field, since it provides immediate information on how to best optimize a particular laser. It also provides an alternate framework in which to view the operation of a mode-locked laser.

Although our approach is general and may be applied to any type of mode-locking mechanism, we chose to focus on FM mode locking. FM mode locking was first demonstrated by Harris and Targ in 1964,[2] making it the second oldest mode-locking technique. Yet no analytic theory capable of adequately predicting pulse parameters exists for these lasers when both dispersion and nonlinearity are present. This shortcoming has become particularly apparent following the first realization of an FM mode-locked fiber laser in 1988.[3]

The time-domain description of AM and FM mode locking was developed in 1970.[4] Although the results from that research are still of great use, it was not until 1986 that the effects of dispersion and nonlinearity were considered in an AM mode-locked laser.[5] This same problem was addressed using soliton perturbation theory almost a decade later.[6] In 2000, another investigation of AM mode locking presented an analytic approach,[7] yet both finite gain bandwidth and third-order dispersion (TOD) were ignored. Although these efforts focused only on AM mode locking in the soliton regime,[5–7] their results have obvious implications for FM mode-locked lasers.[8,9] Yet, only a few analytic investigations have focused on FM mode locking in the presence of dispersion and nonlinearity.[10,11] Indeed, most theoretical investigations of FM mode-locked lasers have primarily relied on numerical modeling to probe the effects of dispersion, nonlinearity, and modulation depth.[9,12,13]

The approach presented in this paper has already been successfully applied to an AM mode-locked laser to obtain a set of rate equations for the pulse parameters.[14] However, FM mode locking has some unique features that set it apart from AM mode locking. For example, FM mode-locked lasers are susceptible to an instability in which mode-locked pulses switch states between the two modulator extrema.[3,15] In the mid 1990's it was shown that this tendency can be suppressed through the introduction of second-order dispersion,[10,16] yet the role of TOD has been considered only recently.[9]

In this paper, we apply the moment method to a generic laser mode locked with an FM modulator and compare our results with numerical simulations based on the full model. In Section 2, the master equation governing mode locking is presented along with the standard pulse solutions commonly expected in various regimes of operation. In Section 3, details behind the moment method are discussed. This method is then applied to an FM mode-locked laser to obtain a set of rate equations for the pulse parameters. Section 4 focuses on steady-state operation and parametric studies. In Section 5, we study the approach to steady state by using a linear stability analysis under the assumption that TOD is negligible. Finally, the

0740-3224/05/122570-11/$15.00

roles of second-order dispersion and TOD are investigated in Section 6 as they pertain to pulse stability.

2. MASTER EQUATION OF MODE LOCKING

If the dispersion and nonlinear lengths[17] of the cavity elements are larger than the round-trip cavity length, L_R, the temporal shape and width of the pulse evolve little during a single round trip (assuming the mode locker's effect on the pulse is weak and losses are minimal). Although an approximate treatment, it is common to model such a system by the so-called master equation of mode locking[5,17]:

$$T_R\frac{\partial A}{\partial T}+\frac{i}{2}(\bar{\beta}_2+i\bar{g}T_2^2)L_R\frac{\partial^2 A}{\partial t^2}-\frac{1}{6}\bar{\beta}_3 L_R\frac{\partial^3 A}{\partial t^3}$$
$$=i\bar{\gamma}L_R|A|^2A+\frac{1}{2}(\bar{g}-\bar{\alpha})L_RA+M(A,t), \quad (1)$$

where $A(T,t)$ is the slowly varying envelope of the electric field, $T=z/v_g$, and v_g is the group velocity. It is important to note there are two time scales in this equation: the time t measured in the frame of the moving pulse and the propagation time T, often called the coarse-grained time.[6] Since we averaged over a single round trip, T is measured in terms of the round-trip time $T_R=L_R/v_g$. It is assumed that the time scale associated with the pulse is sufficiently smaller than T_R so the two times are essentially decoupled. This treatment is valid for most mode-locked lasers for which T_R exceeds 1 ns and pulse widths are typically less than 100 ps.

In rare-earth-doped fibers, as well as in most solid-state materials, the gain medium responds on a time scale much slower than that of the pulse width. As a result, the saturated gain may be approximated as $\bar{g}=\bar{g}_0(1+P_{\mathrm{ave}}/P_{\mathrm{sat}})^{-1}$, where P_{sat} is the saturation power of the gain medium, $\bar{g}_0$ is the average small-signal gain, and P_{ave} represents the average power over one pulse slot of duration T_m, i.e.,

$$P_{\mathrm{ave}}=\frac{1}{T_m}\int_{-T_m/2}^{T_m/2}|A(t,z)|^2\mathrm{d}t. \quad (2)$$

The overbar in Eq. (1) denotes the averaged value of the corresponding parameter; for example, $\bar{\beta}_2$, $\bar{\beta}_3$, $\bar{\alpha}$, and $\bar{\gamma}$ represent the second-order dispersion, TOD, loss, and nonlinearity, respectively, averaged over the cavity length. The gain medium's finite bandwidth is assumed to have a parabolic filtering effect with a spectral full width at half-maximum (FWHM) given by $\Delta_\omega=2/T_2$. $T_m=F_{\mathrm{rep}}^{-1}=m^{-1}T_R$ is the pulse slot, where F_{rep} is the frequency at which our laser is mode locked and m is an integer $\geqslant 1$ representing the harmonic at which the laser is mode locked. For an FM modulator, $M(A,t)=i\Delta_{\mathrm{FM}}\cos[\omega_m(t+t_m)]A$ [in Eq. (1)], where Δ_{FM} is the modulation depth, ω_m is the modulation frequency (assumed to be identical to that of the mode-locked pulse train in this paper, i.e., $\omega_m=2\pi F_{\mathrm{rep}}$), and t_m accounts for any delay between the center of the modulation cycle and the temporal window in which the pulses are viewed.

Although Eq. (1) has no known analytic solution, if the effects of TOD and the mode locker are ignored, this equation reduces to the well-known Ginzburg–Landau equation, which has the following shape-preserving solution[18] known as an autosoliton[17] or a dissipative soliton[19]:

$$A(T,t)=a[\mathrm{sech}(t/\tau)]^{1+iq}\exp(i\kappa T), \quad (3)$$

where

$$\tau^2=\frac{\bar{g}T_2^2+\bar{\beta}_2 q}{\bar{g}-\bar{\alpha}}, \quad (4)$$

$$a^2=\frac{1}{2\bar{\gamma}\tau^2}[(q^2-2)\bar{\beta}_2+3\bar{g}T_2^2q], \quad (5)$$

$$\kappa=-\frac{L_R}{2T_R\tau^2}[(1-q^2)\bar{\beta}_2-2\bar{g}T_2^2q], \quad (6)$$

$$q=\frac{3\bar{\beta}_2}{2\bar{g}T_2^2}\pm\left[\left(\frac{3\bar{\beta}_2}{2\bar{g}T_2^2}\right)^2+2\right]^{1/2}. \quad (7)$$

Despite this analytic solution, cw light is energetically favored by lasers in the absence of a mode locker. When a mode locker is used, the master equation [Eq. (1)] differs from the Ginzburg–Landau equation, and the solution given in Eq. (3) may not hold. Nevertheless, the active fiber will try to impose the autosoliton shape on any pulse circulating in the cavity (in the anomalous dispersion regime). This reasoning was exploited by Haus and Silberberg in their investigation of pulse shortening in AM mode-locked lasers in the presence of dispersive and nonlinear elements.[5]

By completely ignoring the effects of the mode locker and TOD, one immediately limits the generality of the approach; for example, stability is not expected in the absence of the mode locker. Moreover, TOD is known to asymmetrically broaden pulses, thus shifting their arrival time. The mode locker also plays a paramount role: creating and maintaining mode-locked pulses and providing timing information. Thus it is important to include both $\bar{\beta}_3$ and $M(t,A)$ in our analytic treatment. To do so, we assume TOD is weak enough that it primarily affects the arrival time of the mode-locked pulses. This approximation is reasonable for actively mode-locked lasers whose pulse widths are typically in the picosecond regime and whose cavities are dominated by second-order dispersion. Under this assumption, the autosoliton shape is preserved, and we can develop a more robust theory by extending Eq. (3) to allow for both temporal and frequency shifts (ξ and Ω, respectively):

$$A(T,t)=a\{\mathrm{sech}[(t-\xi)/\tau]\}^{1+iq}$$
$$\times\exp[i\Omega(t-\xi)+ikT+i\phi_0]. \quad (8)$$

In the normal dispersion regime ($\bar{\beta}_2>0$), pulses produced by actively mode-locked lasers are usually more consistent with a Gaussian shape[4,10,20] than that of an autosoliton. Therefore, we also consider a chirped Gaussian pulse with complex amplitude

$$A(T,t) = a\{\exp[-(t-\xi)^2/2\tau^2]\}^{1+iq} \times \exp[i\Omega(t-\xi) + ikT + i\phi_0]. \quad (9)$$

In Eq. (9), we have again allowed for both temporal and frequency shifts through ξ and Ω.

One may ask how accurate the pulse-shape assumptions given in Eqs. (8) and (9) are for a realistic mode-locked laser. To answer this question, we numerically solved Eq. (1) using a noise seed (representing spontaneous emission) and the measured parameter values (see Table 1) found for the fiber laser of Ref. 9.[21] Figure 1 compares the steady-state pulse shapes obtained numerically with those of Eqs. (8) and (9). We point out that more than 4000 round trips were required for the pulses to converge to their steady state.

The dashed curves in Fig. 1 show the analytical pulse shapes based on Eqs. (8) and (9). As can be seen in Fig. 1(a), the autosoliton provides a good fit in the anomalous dispersion regime, deviating only in the pulse wings. We verified that this discrepancy is a consequence of finite TOD by setting $\bar{\beta}_3 = 0$ and repeating the simulations. Under these conditions, the numerically predicted pulse shape and the autosoliton shape were almost indistinguishable. In the normal dispersion regime [Fig. 1(b)], the Gaussian fit is accurate about the center of the pulse only. This is due to self-phase modulation, which broadens the center of the pulse in the normal dispersion regime. We verified that as $\bar{\gamma}$ is reduced the accuracy of the Gaussian fit improves until it is almost indistinguishable from the numerical results.

3. MOMENT METHOD

The analytic pulse shapes given in Eqs. (8) and (9) provide an approximate form for the final pulse shape expected after a mode-locked laser reaches its steady state but do not provide any information on how the pulse arrives at that shape nor do they reveal what effect the modulator or TOD has on such a steady-state solution.

To study the pulse evolution process under the influence of Eq. (1), without resorting to full numerical simulations, we employ the moment method.[1] This approach allows us to develop ordinary differential equations that govern the evolution of the pulse parameters. These equations take into account all the terms in Eq. (1), thereby lifting the restriction on the parameter space. However, all of this is based on a knowledge of the exact pulse shape. For this reason, one should carry out numerical simulations with the full model to ensure that the actual pulse shape does not deviate much from the ansatz in the particular region of interest (as we did in Section 2). Experimentally, the results obtained from autocorrelation measurements, electric field reconstruction, or an optical spectrum analyzer may be used to validate a particular ansatz. Although we chose to use the moment method, other techniques such as the variational method or the collective variable method can also be used to obtain ordinary differential equations.

Table 1. Parameter Values Used in This Paper

$\bar{\alpha} = 0.17\ \mathrm{m}^{-1}$	$\bar{\beta}_2 = \pm 1.4\times10^4\ \mathrm{fs}^2/\mathrm{m}$	$\bar{\beta}_3 = 30\times10^4\ \mathrm{fs}^3/\mathrm{m}$
$\bar{\gamma} = 0.012\ (\mathrm{m\ W})^{-1}$	$\bar{g}_0 = 0.55\ \mathrm{m}^{-1}$	$T_2 = 47\ \mathrm{fs/rad}$
$P_{\mathrm{sat}} = 25\ \mathrm{mW}$	$L_R = 4.0\ \mathrm{m}$	$T_R = 40\ \mathrm{ns}$
$\Delta_{\mathrm{FM}} = 0.45$	$F_{\mathrm{rep}} = 10\ \mathrm{GHz}$	$t_m = 0\ \mathrm{ps}$

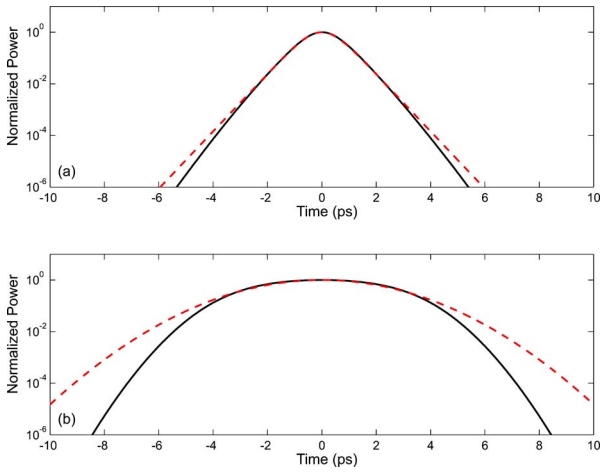

Fig. 1. (Color online) Steady-state pulse shapes in (a) the anomalous dispersion regime and (b) the normal dispersion regime. Plot (a) is fit with the expected autosoliton, and plot (b) is fit with the expected Gaussian.

If we ignore the phase $kT + \phi_0$ in Eqs. (8) and (9), a mode-locked pulse is fully quantified by five parameters: pulse energy E, temporal shift ξ, frequency shift Ω, chirp q, and width τ. In the moment method, the five parameters are defined in terms of the temporal pulse profile via[22,23]

$$E(T) = \int_{-\infty}^{\infty} |A(T,t)|^2 \mathrm{d}t, \quad (10)$$

$$\xi(T) = \frac{1}{E}\int_{-\infty}^{\infty} t|A(T,t)|^2 \mathrm{d}t, \quad (11)$$

$$\Omega(T) = \frac{i}{2E}\int_{-\infty}^{\infty}\left[A^*\frac{\partial A}{\partial t} - A\frac{\partial A^*}{\partial t}\right]\mathrm{d}t, \quad (12)$$

$$q(T) = \frac{i}{E}\int_{-\infty}^{\infty}(t-\xi)\left[A^*\frac{\partial A}{\partial t} - A\frac{\partial A^*}{\partial t}\right]\mathrm{d}t, \quad (13)$$

$$\tau^2(T) = \frac{2C_3}{E}\int_{-\infty}^{\infty}(t-\xi)^2|A(T,t)|^2 \mathrm{d}t, \quad (14)$$

where the constant C_3, defined later in this section, converts the root-mean-square width into pulse width τ. To investigate how the five pulse parameters evolve during propagation, we differentiate Eqs. (10)–(14) with respect to T, yielding

$$\frac{\mathrm{d}E}{\mathrm{d}T} = \int_{-\infty}^{\infty}\left[A^*\frac{\partial A}{\partial t} + A\frac{\partial A^*}{\partial T}\right]\mathrm{d}t, \quad (15)$$

$$\frac{\mathrm{d}\xi}{\mathrm{d}T} = -\frac{1}{E}\frac{\mathrm{d}E}{\mathrm{d}T}\xi + \frac{1}{E}\int_{-\infty}^{\infty} t\left[A^*\frac{\partial A}{\partial t} + A\frac{\partial A^*}{\partial t}\right]\mathrm{d}t, \quad (16)$$

$$\frac{d\Omega}{dT} = -\frac{1}{E}\frac{dE}{dT}\Omega + \frac{i}{2E}\int_{-\infty}^{\infty}\left[\frac{\partial}{\partial T}\left(A^*\frac{\partial A}{\partial T}\right) - \frac{\partial}{\partial T}\left(A\frac{\partial A^*}{\partial t}\right)\right]dt, \quad (17)$$

$$\frac{dq}{dT} = -\frac{1}{E}\frac{dE}{dT}q + \frac{i}{E}\int_{-\infty}^{\infty}(t-\xi)\left[\frac{\partial}{\partial T}\left(A^*\frac{\partial A}{\partial t}\right) - \frac{\partial}{\partial T}\left(A\frac{\partial A^*}{\partial t}\right)\right]dt, \quad (18)$$

$$\tau\frac{d\tau}{dT} = -\frac{1}{2E}\frac{dE}{dT}\tau^2 + \frac{C_3}{E}\int_{-\infty}^{\infty}(t-\xi)^2\left[A^*\frac{\partial A}{\partial T} + A\frac{\partial A^*}{\partial T}\right]dt. \quad (19)$$

The final step consists of substituting $\partial A/\partial T$ from Eq. (1) into Eqs. (15)–(19) and integrating over t after assuming a pulse shape.

For the two pulse shapes, given in Eqs. (8) and (9), all these integrals can be done analytically. After some algebra, we obtain the following equations for the evolution of the five pulse parameters:

$$\frac{T_R}{L_R}\frac{dE}{dT} = (\bar{g}-\bar{\alpha})E - \frac{\bar{g}T_2^2}{2\tau^2}[C_0(1+q^2)+2\Omega^2\tau^2]E, \quad (20)$$

$$\frac{T_R}{L_R}\frac{d\xi}{dT} = \bar{\beta}_2\Omega - \bar{g}T_2^2 q\Omega + \frac{\bar{\beta}_3}{4\tau^2}[C_0(1+q^2)+2\Omega^2\tau^2], \quad (21)$$

$$\frac{T_R}{L_R}\frac{d\Omega}{dT} = -C_0\frac{\bar{g}T_2^2}{\tau^2}(1+q^2)\Omega + \frac{\Delta_{FM}\omega_m}{L_R}\Psi_0 \times \sin[\omega_m(\xi - t_m)], \quad (22)$$

$$\frac{T_R}{L_R}\frac{dq}{dT} = \frac{\bar{\beta}_2}{\tau^2}[C_0(1+q^2)+2\Omega^2\tau^2] - \frac{\bar{g}T_2^2}{\tau^2}q[C_1(1+q^2) + 2\Omega^2\tau^2] + C_2\frac{\bar{\gamma}E}{\sqrt{2\pi}\tau} + \frac{\bar{\beta}_3\Omega}{\tau^2}\left[\frac{3}{2C_0}(1+q^2) + \Omega^2\tau^2\right] + \frac{\Delta_{FM}\omega_m\tau}{L_R}\Psi_1\cos[\omega_m(\xi - t_m)], \quad (23)$$

$$\frac{T_R}{L_R}\frac{d\tau}{dT} = C_3\frac{\bar{\beta}_2}{\tau}q + C_3\frac{\bar{\beta}_3}{\tau}q\Omega + C_0C_3\frac{\bar{g}T_2^2}{2\tau}(C_4 - q^2), \quad (24)$$

where the constants C_n ($n=0$ to 4) are introduced such that they all equal 1 for a Gaussian pulse. In the case of an autosoliton, $C_0=2/3$, $C_1=1/3$, $C_2=\sqrt{2\pi}/3$, $C_3=6/\pi^2$, and $C_4=2$. We have also introduced $\Psi_0=\exp(-\omega_m^2\tau^2/4)$ and $\Psi_1=\omega_m\tau\Psi_0$ for the Gaussian pulse. For the autosoliton, $\Psi_0=(\pi\omega_m\tau/2)\mathrm{csch}(\pi\omega_m\tau/2)$ and $\Psi_1=[\pi\coth(\pi\omega_m\tau/2)-2/(\omega_m\tau)]\Psi_0$.

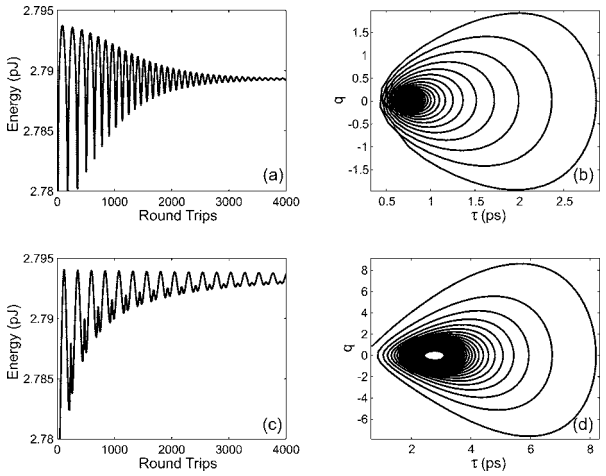

Fig. 2. Evolution of pulse energy E, width τ, and chirp q over multiple round trips in the case of anomalous (top row) and normal (bottom row) dispersion.

Equations (20)–(24) are analogous to the traditional rate equations used for cw lasers, and we refer to them as the FM mode-locking rate equations. They were numerically solved in a fraction of the time required to solve the original equation [Eq. (1)] by using the fourth-order Runge–Kutta method and the parameters found in Table 1.[21] Figure 2 displays how pulse energy E, width τ, and chirp q change from one round trip to the next when seeded with the initial values $E(0)=1$ fJ, $\xi(0)=0$ fs, $\Omega(0)=0$ GHz, $\tau(0)=0.5$ ps, and $q(0)=0$. The plots for $\tau(T)$ and $q(T)$ were combined into one phase-space plot by our plotting q as a function of τ. As can be seen in the first column of Fig. 2, pulse energy increases from 1 fJ to $\approx$2.8 pJ in less than 100 round trips but then exhibits damped oscillations as it evolves over thousands of round trips. In fact, more than 4000 round trips are necessary before the pulse parameters converge to their steady-state values, a situation similar to that found when we performed the numerical simulations to create Fig. 1. The steady-state values obtained through our rate-equation approach deviate from the values obtained by directly solving Eq. (1) by $<3\%$ in the anomalous dispersion regime and $<12\%$ in the normal dispersion regime. This agreement justifies the use of the moment method and the pulse shapes assumed. Note that in the case of normal dispersion [Fig. 2(d)] the pulse has not reached a final steady state even after 4000 round trips. In general, the approach to steady state takes longer when the residual cavity dispersion is normal, since the modulator's compression effect must balance both dispersive and nonlinear broadening. In fact, it has even been reported that a train of well-separated mode-locked pulses could not be experimentally realized at a high repetition rate in this regime.[10,16] Of course, this result depends on the laser parameters: In the presence of nonlinearity, it indicates that stronger modulation depths are required to obtain mode locking in the normal dispersion regime.

4. STEADY-STATE PULSE CHARACTERISTICS

In the preceding section, the evolution of pulse parameters toward their steady-state values was studied by our

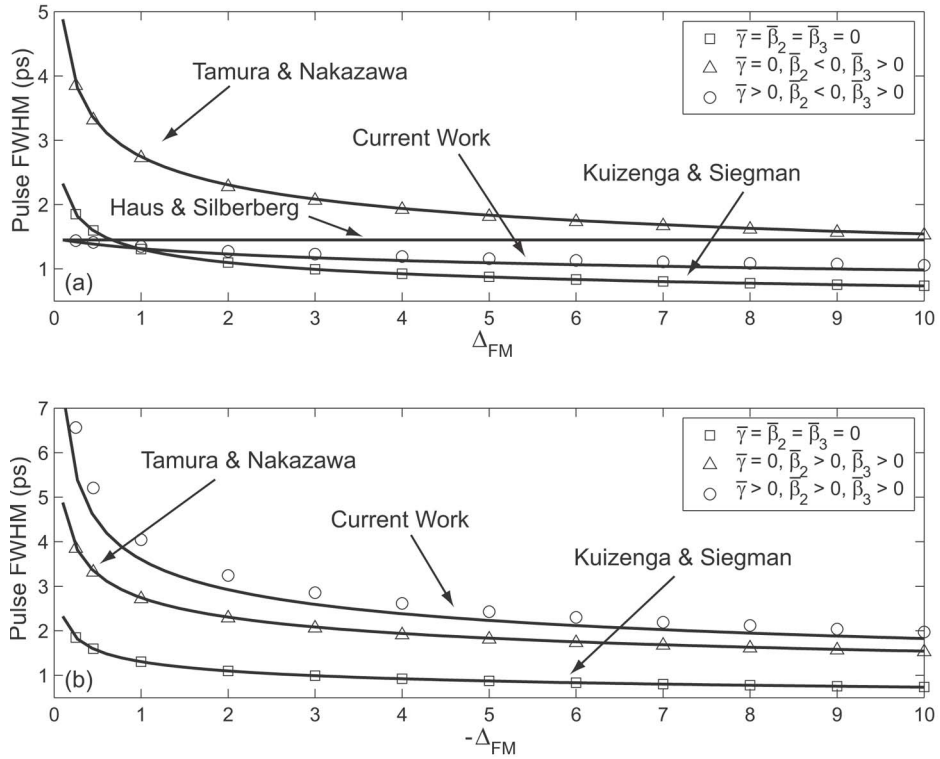

Fig. 3. Pulse width predicted by our theory as a function of modulation depth in the (a) anomalous and (b) normal dispersion regimes. In each case, we compare our predictions with numerical simulations and with the theories given in Refs. 4 and 5 (when $\bar{\beta}_2 < 0$), and 10.

solving the mode-locking rate equations numerically. Although good agreement was obtained, the true strength of our approach lies in predicting the steady-state values for mode-locked pulses. Assuming that the mode-locked laser has reached a steady state, the pulse parameters may be determined quasi-analytically by one's setting the derivatives to zero in Eqs. (20)–(24). The resulting system of nonlinear algebraic equations is easily solved using the Newton–Raphson technique. Since this scheme converges quickly, given a reasonable initial guess, parametric studies may be performed effortlessly.

Figure 3 demonstrates the strength of our approach by studying the effect of modulation depth on pulse width. To put this research in perspective, our results are presented, along with those based on previous theories, in both anomalous and normal dispersion regimes. In both cases, we consider a linear nondispersive cavity (squares), a linear dispersive cavity (triangles), and a cavity with both nonlinearity and dispersion (circles). Data points marked with symbols were obtained using the full numerical model [Eq. (1)], whereas solid curves were generated using the corresponding analytic treatment in each case. The theory developed by Kuizenga and Siegman[4] predicts the pulse width when dispersion and nonlinearity are neglected. With the inclusion of dispersion,[4] an extended version of this theory used by Tamura and Nakazawa[10] predicts the pulse width. Haus and Silberberg's theory predicts the pulse parameters when both nonlinearity and anomalous dispersion are included; yet, it fails to include TOD or modulation depth and is invalid in the normal dispersion regime.[5] As a result, only the theory developed in this paper is found to be in good agreement with the numerical results in the presence of both nonlinearity and dispersion. Moreover, our theory reproduces all the prior results in the appropriate limits.

A noteworthy feature of Fig. 3(a) is that for modulation depths $\Delta_{FM} < 0.9$ the mode-locked pulse experiences soliton pulse compression,[3,5,6,24–26] since the pulse width becomes shorter than that predicted by the simplified theory of Ref. 4. For $\Delta_{FM} > 0.9$, the modulator plays an increasingly dominant role. Nevertheless, excellent agreement is obtained between the simulations and our theory even for large modulation depths (1.3% error for $\Delta_{FM} = 0.25$, 7% error for $\Delta_{FM} = 10$). Conversely, the agreement in Fig. 3(b) is seen to increase with the modulation depth (15% error for $\Delta_{FM} = -0.25$, 7% error for $\Delta_{FM} = -10$). This behavior can be understood by one's noting that the modulator's preferred shape is a Gaussian.[4,10] As a result, our accuracy improves with modulation depth in the normal dispersion regime but deteriorates in the anomalous dispersion regime.

An important question we can answer with our semianalytic approach [Eqs. (20)–(24)] is how the residual cavity dispersion $\bar{\beta}_2$ and the nonlinear parameter $\bar{\gamma}$ affect the final steady-state pulses. Figure 4 shows how the pulse parameters τ, q, ξ, and Ω vary with $\bar{\beta}_2$ in the anomalous (top row) and normal (bottom row) dispersion regimes. The shortest pulses are obtained in the case of anomalous dispersion for small values of $|\bar{\beta}_2|$: Pulse FWHM reduces to below 1 ps for $|\bar{\beta}_2| < 0.01$ ps^2/m. In contrast, pulse FWHM exceeds 4 ps in the normal dispersion case and increases as $\bar{\beta}_2$ increases. Notice that, when $|\bar{\beta}_2| < 0.01$ ps^2/m, the pulse position shifts because TOD plays

an increasing role in the laser (especially in the anomalous dispersion regime where the pulse spectrum is broader). Figure 5 shows the effect on the pulse parameters when the nonlinear parameter $\bar{\gamma}$ is varied for a fixed value of $\bar{\beta}_2$; dispersion is anomalous for the top row and normal for the bottom row. In the case of anomalous dispersion, the pulse becomes shorter for larger values of $\bar{\gamma}$. The situation is opposite in the case of normal dispersion. Figure 5 also reveals the interesting result that chirp, q, is essentially independent of $\bar{\gamma}$.

5. APPROXIMATE STEADY-STATE PULSE PARAMETERS

In an effort to obtain a semianalytic result, we turn our attention to the case in which the effect of TOD is negli-

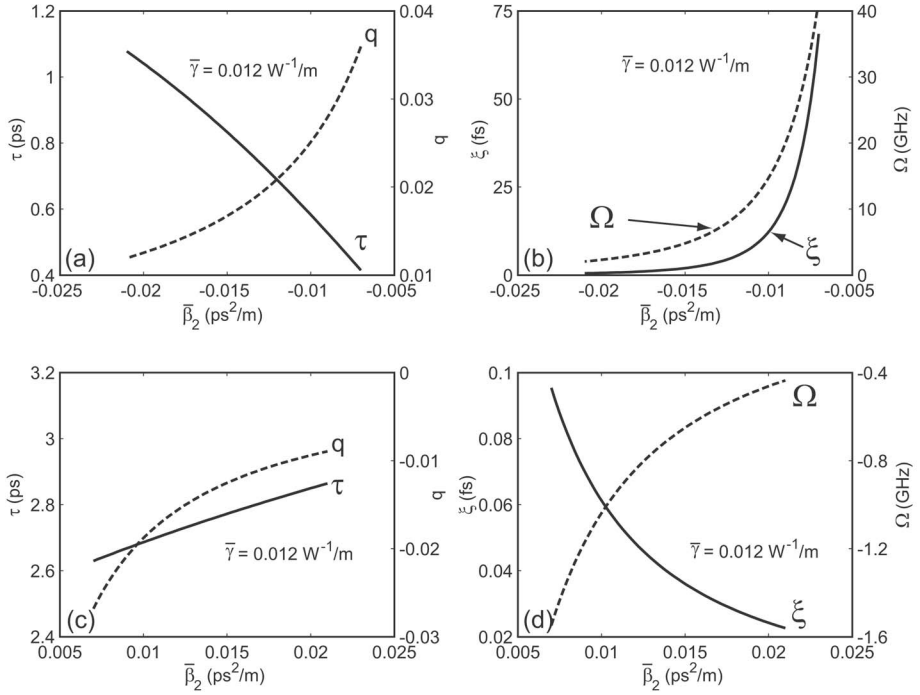

Fig. 4. Steady-state pulse width τ, chirp q (left column), temporal shift ξ, and frequency shift Ω (right column) in the anomalous (top row) and normal (bottom row) dispersion regimes.

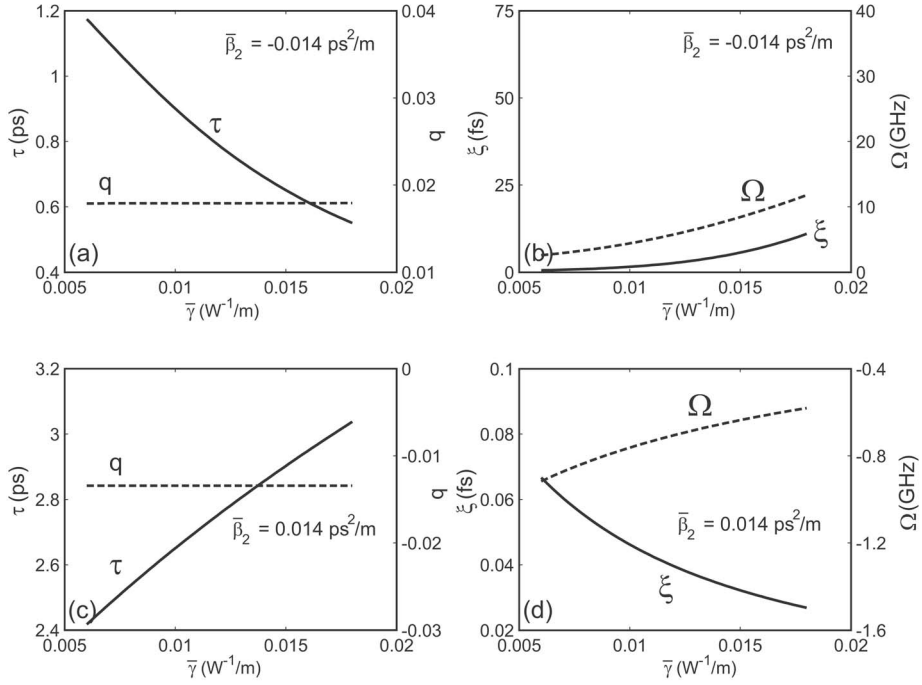

Fig. 5. Same as Fig. 4 except the pulse parameters are plotted as a function of the nonlinear parameter.

gible, as is frequently the case for actively mode-locked lasers. Under such conditions, both ξ and $\Omega=0$ in the steady state, and Eqs. (20)–(24) reduce to a set of three equations for E, q, and τ. After a large number of round trips, we can set the derivatives to zero and obtain

$$\frac{T_R}{L_R}\frac{dE}{dT}=\bar{g}_{ss}-\bar{\alpha}-\frac{\bar{g}_{ss}T_2^2}{2\tau_{ss}^2}C_0(1+q_{ss}^2)=0, \tag{25}$$

$$\frac{T_R}{L_R}\frac{dq}{dT}=\frac{\bar{\beta}_2}{\tau_{ss}^2}C_0(1+q_{ss}^2)-\frac{\bar{g}_{ss}T_2^2}{\tau_{ss}^2}q_{ss}C_1(1+q_{ss}^2)+C_2\frac{\bar{\gamma}E_{ss}}{\sqrt{2\pi}\tau_{ss}}+\frac{\Delta_{FM}\omega_m\tau_{ss}}{L_R}\Psi_1=0, \tag{26}$$

$$\frac{T_R}{L_R}\frac{d\tau}{dT}=C_3\bar{\beta}_2q_{ss}+C_0C_3\frac{\bar{g}_{ss}T_2^2}{2}(C_4-q_{ss}^2)=0. \tag{27}$$

If we go one step further and assume that $\bar{g}_{ss}$ and E_{ss} are known quantities, as assumed in previous analytic studies,[4,5,10] we are able to obtain, for what we believe to be the first time, a fully analytic description of FM mode-locked lasers in the presence of dispersion, nonlinearity, and modulation depth. Equation (27) can be written as $q^2-2dq-C_4=0$, where $d=\bar{\beta}_2/(C_0\bar{g}_{ss}T_2^2)$ is a dimensionless dispersion parameter. The steady-state chirp parameter is then given by

$$q_{ss}=d\pm\sqrt{d^2+C_4}, \tag{28}$$

and the pulse width is found by one's solving Eq. (26) for τ_{ss}. It is imperative to point out that Eq. (26) predicts multiple solutions are possible, in principle, for a given set of laser parameters. The stability of these solutions is discussed in detail in Section 6. Here we point out that only one solution dominates in practice, and we focus on it for the time being. Interestingly, Eq. (28) shows that chirp is independent of the nonlinear parameter $\bar{\gamma}$. It is also independent of the modulation parameters, a somewhat surprising feature for FM modulation, which affects the optical phase directly. Despite the fact that TOD was ignored, this finding agrees with Fig. 5, in which all effects were included yet chirp was essentially independent of $\bar{\gamma}$.

Equation (25) predicts the extent to which the mode-locking threshold exceeds the cw value $\bar{\alpha}$. More specifically,

$$\bar{g}_{ss}=\bar{\alpha}\left[1-\frac{C_0T_2^2}{2\tau_{ss}^2}(1+q_{ss}^2)\right]^{-1}\approx\bar{\alpha}+\frac{C_0T_2^2\bar{\alpha}}{2\tau_{ss}^2}(1+q_{ss}^2). \tag{29}$$

Since $\sqrt{1+q_{ss}^2}/\tau_{ss}$ is related to pulse spectral width, this equation has a simple interpretation: The threshold gain for an FM mode-locked laser exceeds the total cavity loss by an amount that depends on the fraction of the gain spectrum occupied by the mode-locked pulse spectrum. A similar result is obtained for AM mode locking, although modulator loss is important in that case.[14]

As noted in Section 4, our theory reproduces previously known results in the appropriate limits. If the effect of the modulator is ignored, by setting $\Delta_{FM}=0$, we find that our results collapse to those of Ref. 5 in the anomalous dispersion regime. If nonlinearity is ignored, by setting $\bar{\gamma}=0$, we obtain the results of Ref. 10. If we go one step further and also neglect second-order dispersion and TOD, we should recover the results of Ref. 4. Under such conditions, $d=0$ and $q_{ss}=\pm\sqrt{C_4}$. Of course, in the absence of nonlinearity, we expect a chirped Gaussian pulse and $C_4=1$, yielding $q_{ss}=\pm1$. The temporal FWHM (after Taylor expansion of the Ψ_1 term) of the Gaussian pulse is then simply given by

$$\tau_{FWHM}=2[\sqrt{2}\ln(2)]^{1/2}\left(\frac{\bar{g}_{ss}L_R}{\Delta_{FM}}\right)^{1/4}\left(\frac{T_2}{\omega_m}\right)^{1/2}. \tag{30}$$

This equation is identical to the result obtained in Ref. 4.

Expressions (28) and (29) are coupled; however, in most practical cases $\bar{g}_{ss}$ exceeds $\bar{\alpha}$ by $<0.5\%$. Using the parameter values of Table 1 and solving Eqs. (26)–(28), we find that $\bar{g}_{ss}=\bar{\alpha}+2.02\times10^{-4}\ m^{-1}$, confirming that this is indeed true here. Therefore, to facilitate a fully analytic approach, we assume $\bar{g}_{ss}\approx\bar{\alpha}$, which introduces only a slight penalty in accuracy. Under this assumption, our rate-equation approach predicts a steady-state chirp of $q_{ss}=0.0179$ and a pulse width of $\tau_{ss}=0.787$ ps (FWHM $=1.76\tau_{ss}$). These values agree well with those found by one's directly solving Eq. (1) ($\tau_{ss}=0.798$ ps, $q_{ss}=0.0174$). The good agreement found here justifies the $\bar{g}_{ss}\approx\bar{\alpha}$ approximation as well as the simplified approach of ignoring the ξ and Ω equations adopted in this section.

The mode-locking rate equations can also provide information on the approach to the steady state, which frequently involves relaxation oscillations as seen in Fig. 2. We have performed a linear stability analysis on Eqs. (26) and (27) to obtain the following expression for the relaxation-oscillation frequency associated with small perturbations:

$$\omega_r=\frac{L_R}{\tau_0T_R}\sqrt{BC-D^2}, \tag{31}$$

where

$$B=-\frac{C_3}{\tau_{ss}}(\bar{\beta}_2-C_0\bar{g}T_2^2q_{ss}), \tag{32}$$

$$C=\frac{C_2\bar{\gamma}E}{\sqrt{2\pi}}+\frac{4\Delta_{FM}\omega_m^2\tau_{ss}^3}{C_3L_R}, \tag{33}$$

$$D=\frac{1}{2\tau_{ss}}[2\bar{\beta}_2C_0q_{ss}-\bar{g}T_2^2C_1(1+3q_{ss}^2)]. \tag{34}$$

However, to obtain these results in a compact form it was necessary to Taylor expand Ψ_1 to first order in $\tau=\tau_{ss}$. Equation (31) predicts an oscillation frequency of 230 kHz by using the parameters of Table 1 and $\bar{g}_{ss}\approx\bar{\alpha}$. This result agrees well with the 235 kHz value obtained through numerically solving Eq. (1), again justifying the use of the approximations made.

6. STABILITY OF STEADY-STATE SOLUTIONS

It is well known that FM mode-locked lasers can operate with pulses at either modulator extremum.[3,4,15] These two possible operating states correspond to $\omega_m(t-t_m)=0$ and $\omega_m(t-t_m)=\pi$; they also make FM mode-locked lasers prone to a switching instability.[4,10,15,16] Our theory predicts pulse formation at both of these locations, as it should. For example, pulse chirp q in Eq. (28) has two possible steady-state values. In a linear nondispersive cavity, a single pulse width τ is associated with each value of chirp q.[4] However, the presence of dispersive and nonlinear terms in Eq. (26) allows multiple solutions for τ for each value of q.

Figure 6 shows how the two solutions for q vary with the residual cavity dispersion $\bar{\beta}_2$ [via Eq. (28)]. The curve labeled $\Delta_{\mathrm{FM}}>0$ represents the chirp imposed on the pulse located at the $\omega_m(t-t_m)=0$ modulator extremum, and the curve labeled $\Delta_{\mathrm{FM}}<0$ represents the chirp imposed on the pulse at the other extremum. In a linear nondispersive cavity $q=\pm 1$. However, Fig. 6 shows that by one's introducing residual second-order dispersion into the cavity the pulse chirp in FM mode-locked lasers can be reduced significantly to $q\approx 0$. This result, which could be inferred from Figs. 4 and 5, is also in agreement with the experimental findings of many groups.[3,10,16,20,24,27] Another interesting feature to note is that the two states are temporally separated from each other: As cavity dispersion is increased from anomalous to normal, a pulse must temporally shift to align itself with the modulator's other extrema. Two shifting mechanisms have previously been identified through numerical simulations: shifting initiated through noise (or growth from pulse wings) and shifting initiated by TOD.[9]

In Section 5, we focused on the $\Delta_{\mathrm{FM}}>0$ case in the anomalous dispersion regime (characterized by $\tau=0.787$ ps and $q=0.0179$). In this section, we start with the physical explanation as to why one state dominates in an FM mode-locked laser; we then use the moment method to map out the stable and unstable points of operation in a visually intuitive fashion. Focusing again on the anomalous dispersion regime and the laser whose parameters are given in Table 1, we find that the chip parameter can be either small ($q=0.0179$) or large ($q=-111.73$). When $\Delta_{\mathrm{FM}}=0.45$, we find a solution ($\tau=0.787$ ps) only for the $q=0.0179$ case. The situation is much more complicated for $\Delta_{\mathrm{FM}}=-0.45$ [i.e., $\omega_m(t-t_m)=\pi$]. We now find five possible solutions, each with a different pulse width. For $q=0.0179$, three solutions are found: $\tau=0.94$, 1.5, and 149 ps. When $q=-111.73$, two solutions are found: $\tau=16.2$ and 93.3 ps. Although these results were obtained using Eqs. (26) and (28), they were also verified by our solving the full system of Eqs. (20)–(24) in the steady state. Only one among these five potential solutions for $\Delta_{\mathrm{FM}}=-0.45$ is likely to be stable. Indeed, a stability analysis reveals that all three states found for $q=0.0179$ are unstable (a simple way to perform such an analysis is discussed later in this section). Among the remaining two states, the solution with $\tau=93.3$ ps is not physical at our 10 GHz repetition rate, since these pulses extend outside the pulse slot. Therefore, we are left with only one stable solution when $\Delta_{\mathrm{FM}}=-0.45$: $\tau=16.2$ ps and $q=-111.73$.

Having found a unique solution for positive and negative values of Δ_{FM}, we now investigate their relative stability. The pulse spectra are quite different for these two solutions. Indeed, the spectral FWHM is 0.23 THz when $\Delta_{\mathrm{FM}}=0.45$ but broadens to 2.17 THz when $\Delta_{\mathrm{FM}}=-0.45$. Pulses with narrower spectra will clearly incur less loss due to the finite gain bandwidth [see expression (29)] and any other wavelength-dependent loss in the cavity; they are therefore favored by the laser. For this reason, we call this solution dominant and the other, higher loss, solution secondary. The dominant mode-locked pulses always form under modulator cycles satisfying the condition $\Delta_{\mathrm{FM}}\bar{\beta}_2\leqslant 0$. This behavior, first alluded to by Kuizenga and Siegman,[4] was investigated in a series of papers by Nakazawa and co-workers[10,16,20,27] in the mid 1990's. Furthermore, Tamura and Nakazawa's argument that the switching tendency is suppressed in the presence of strong dispersion[10] is verified by Fig. 6 if one recalls that the pulse spectra is proportional to $\sqrt{1+q^2}/\tau$ and then applies the spectral filtering argument.

We now turn our attention to the effects of dispersion on pulse stability, as predicted by the moment method. Equations (20)–(24) reveal that changes in ξ and Ω do not have a strong effect on the other pulse parameters so long as $2\Omega\tau\ll C_0$. Figures 4 and 5 show that $\Omega\tau<10^{-2}$ over a broad range of operating conditions. Since $C_0\leqslant 1$, we can assume pulse energy, width, and chirp are approximately independent of Ω and ξ. Doing so allows us to solve Eq. (22) analytically and obtain

$$\Omega(T)=\frac{\Delta_{\mathrm{FM}}\omega_m\tau^2}{C_0L_R\bar{g}T_2^2(1+q^2)}\Psi_0\sin[\omega_m(\xi-t_m)]+C\exp\left[-\frac{C_0L_R\bar{g}T_2^2(1+q^2)}{\tau^2T_R}T\right], \tag{35}$$

where C is an integration constant. Noting the second term vanishes for $T\gg T_R$, we substitute Eq. (35) into Eq.

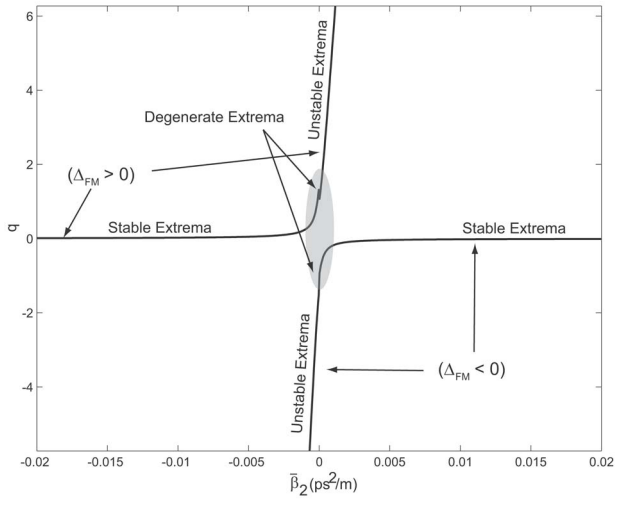

Fig. 6. Chirp as a function of average dispersion $\bar{\beta}_2$ from Eq. (28).

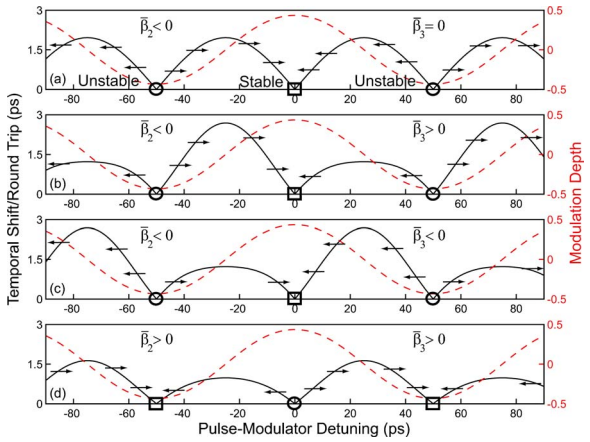

Fig. 7. (Color online) Temporal shift per round trip as a function of pulse-modulator detuning using the dominant pulse parameters ($\tau=0.787$ ps, $q=0.0179$). These figures identify the stable (squares) and unstable (circles) operating locations as well as the strength and direction of the pulse velocity for the following cases: (a) $\bar{\beta}_2<0$ and $\bar{\beta}_3=0$, (b) $\bar{\beta}_2<0$ and $\bar{\beta}_3>0$, (c) $\bar{\beta}_2<0$ and $\bar{\beta}_3<0$, and (d) $\bar{\beta}_2>0$ and $\bar{\beta}_3>0$. The imaginary part of the modulator's signal is plotted by the dashed curve to aid in location identification for a fixed modulation depth of $\Delta_{\mathrm{FM}}=0.45$.

(21) to obtain the following equation for $T_R\mathrm{d}\xi/\mathrm{d}T$, a quantity we refer to as the temporal shift per round trip of the pulse relative to the modulation cycle:

$$T_R\frac{\mathrm{d}\xi}{\mathrm{d}T}=L_R(\bar{\beta}_2-\bar{g}T_2^2q)\frac{\Delta_{\mathrm{FM}}\omega_m\tau^2}{C_0L_R\bar{g}T_2^2(1+q^2)}\Psi_0\sin[\omega_m(\xi-t_m)]$$
$$+L_R\frac{\bar{\beta}_3}{4\tau^2}\left\{C_0(1+q^2)+\frac{2\Delta_{\mathrm{FM}}^2\omega_m^2\tau^6}{C_0^2L_R^0\bar{g}^2T_2^4(1+q^2)^2}\Psi_0^2\sin^2[\omega_m(\xi-t_m)]\right\}. \quad (36)$$

By varying the detuning between the pulse location and the modulator extrema, $\xi-t_m$, we map out the magnitude of this shift, along with arrows indicating its direction, in Fig. 7, where four different regimes are shown for the dominant mode-locked solution ($\tau=0.787$ ps and $q=0.0179$). In Fig. 7, the stable and unstable locations are identified with squares and circles, respectively, and they occur at pulse-modulator detunings where the pulse does not experience a temporal shift. The stable points occur at locations where a slight perturbation results in a temporal shift that restores the initial state. Unstable states, on the other hand, are identified where a slight perturbation sends the pulse to a different state. TOD manifests itself by making the magnitude of $\mathrm{d}\xi/\mathrm{d}T$ asymmetric about the stable and unstable points depending on its sign as can be seen by comparing Figs. 7(a)–7(c). In Fig. 7(a), where $\bar{\beta}_3=0$, the magnitude of the temporal shift experienced by the pulse is symmetric about the stable and unstable operating points. In contrast, pulse shift becomes asymmetric in Figs. 7(b) and 7(c), where $\bar{\beta}_3\neq 0$. Depending on the sign of $\bar{\beta}_3$, pulses temporally shift faster in one direction; this intuitive result was previously reported through numerical simulations.[9]

Equation (36) also provides a simple way to investigate the stability of the pulse solutions by using the values obtained for τ and q in this equation and plotting the results. These plots immediately reveal that the three $\Delta_{\mathrm{FM}}<0$ and $q=0.0179$ solutions (previously noted) are unstable; full numerical simulations of Eq. (1) were also used to verify this claim.

To demonstrate what happens in the normal dispersion regime, Fig. 7(d) shows the case $\bar{\beta}_2>0$. As can be seen in the figure, the $\Delta_{\mathrm{FM}}<0$ extremum of the modulation cycle represents the stable location for pulse formation. We point out that this result agrees with the simple rule $\Delta_{\mathrm{FM}}\bar{\beta}_2<0$ and has been confirmed numerically.

With the Gaussian ansatz, temporal shift per round trip can also be plotted for a nondispersive linear cavity, by setting $\bar{\beta}_2=\bar{\beta}_3=\bar{\gamma}=0$ and using Eq. (36). In this case, pulse width and chirp are found to be $\tau=0.7432$ ps and $q=\pm 1$ by using Eqs. (28) and (30). The absence of dispersion and nonlinearity has caused the dominant and secondary solutions to collapse into one solution differing only in the sign of the chirp. As a consequence, neither solution dominates, and we expect pulses to simultaneously exist under both modulator extrema. Experimentally, however, the laser randomly switches through noise-induced perturbations between the two states; to our knowledge they have not been found to coexist.[15]

If the parameters of the secondary pulse ($\tau=16.2$ ps and $q=-111.73$) are used instead of those of the dominant pulse, the results shown in Fig. 8 are obtained. Figures 8(a) and 8(b) show that the secondary pulses exist at the opposite modulator extrema as that of the dominant pulses, as expected. By comparing Figs. 8(a) and 8(b) with Figs. 7(a) and 7(b), we find the temporal shifts experienced by the pulses during a single round trip are much stronger for dominant pulses than those experienced by secondary pulses. That is, our theory shows dominant pulses are bound more tightly to their stable operating

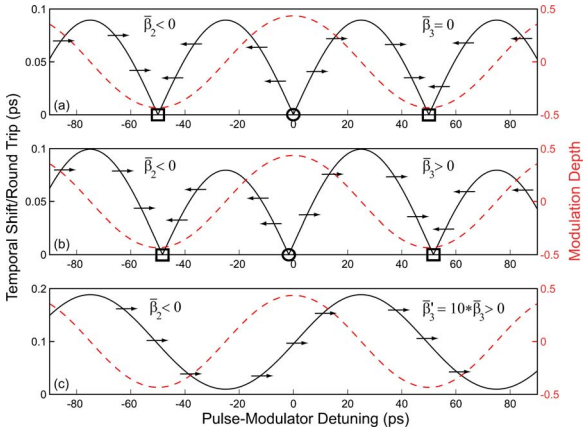

Fig. 8. (Color online) Temporal shift per round trip as a function of pulse-modulator detuning using the secondary pulse parameters ($\tau_0=16.2$ ps, $q_0=-111.73$). These figures identify the stable (squares) and unstable (circles) operating locations as well as the strength and direction of the pulse velocity for the following cases: (a) $\bar{\beta}_2<0$ and $\bar{\beta}_3=0$, (b) $\bar{\beta}_2<0$ and $\bar{\beta}_3>0$, and (c) result of large TOD on stable pulses. The imaginary part of the modulator's signal is plotted by the dashed curve to aid in location identification for a fixed modulation depth of $\Delta_{\mathrm{FM}}=0.45$.

points than secondary pulses. This is expected on physical grounds and is a direct consequence of second-order dispersion and spectral filtering.

Once again we see that TOD has added an asymmetry to the strength of the pulse shift by comparing Figs. 8(a) and 8(b). Since the laser needs a finite amount of time to switch between states, it becomes possible to observe the secondary state, at least through numerical simulations. Despite the fact that this state is not dominant, numerical evidence for its transient existence has been confirmed by consideration of the effect of an abrupt half-clock-cycle phase shift in the driving electronics on the dominant pulse.[9] It was found that the pulse shifts under the influence of the TOD, resynchronizing with the stable modulation extrema, while essentially retaining its shape. If the TOD is weak, or the pulse is unable to survive the perturbation intact, it broadens instead of shifting. In Ref. 9 the pulse broadened but then became trapped in a local potential until it was destabilized by the reformation of the dominant pulse, which was seeded by the pulse wings and noise. The transient state found in that study is just what we have referred to as the secondary state here.

According to the current paper, it follows from Fig. 7(b) that if the pulse survives the modulator-induced perturbation and retains its width and chirp, its center would be subject to the temporal shift identified in that figure. To clarify our meaning, consider what happens if a steady-state mode-locked pulse located at $\xi - t_m = -48$ ps is subjected to a π phase shift through the driving electronics. According to Fig. 7(b), the pulse would physically shift to relocate itself under the correct modulation cycle ($\xi - t_m = 0$ ps). If, however, the pulse cannot survive the perturbation, it will broaden while remaining centered on $\xi - t_m = -48$ ps. Instead of broadening unabated, it will become trapped in a local potential associated with the secondary state [$\tau = 16.2$ ps and $q = -111.73$, see Fig. 8(b)]. At this point, the pulse is locally stable. The laser will return to its dominant steady-state mode-locked pulse only when the secondary state is destabilized by the laser's choice to operate in the lower-loss state located at $\xi - t_m = 0$ ps (in this case, the stable pulse grows from noise). By an increase in pulse energy, the pulse may remain intact through solitonic shaping, despite the modulator-induced perturbation. Such a pulse would then switch out of the shallow secondary-state potential. Comparing Figs. 7(b) and 7(c), we further expect that the direction of the pulse-center shift should depend on the sign of the TOD. All of these effects were numerically observed and explored in Ref. 9.

Finally, Fig. 8(c) answers the question as to what happens when TOD is increased. In this case, TOD was increased by a factor of 10 to $\bar{\beta}_3 = 300 \times 10^4$ fs^3/m, and we find that mode-locked operation is no longer possible, since the shifting effect of the TOD is stronger than the modulator's ability to synchronize the pulses.

7. CONCLUSION

In conclusion, by applying the moment method to the master equation governing pulse formation in mode-locked fiber lasers, we derived a set of five coupled ordinary differential equations for the pulse parameters. These equations can be solved rapidly on a computer by using well-known techniques. Furthermore, they reduce to algebraic equations in the steady state, which enables one to quickly obtain solutions. This method was applied to an FM mode-locked laser, allowing us to obtain analytic expressions for pulse parameters. We were able to map out the dynamics experienced by mode-locked pulses and predict the stable and unstable operating locations relative to the modulator's cycle. This approach also allowed us to study the effects of second- and third-order dispersions on pulse stability.

The rate-equation approach used in this paper is likely to be useful in the field of mode-locked lasers. Moreover, the analytic results obtained by its application to standard mode-locking techniques appear to be a useful tool for experimentalists.

ACKNOWLEDGMENTS

This study was supported by the U.S. Department of Energy (DOE) Office of Inertial Confinement Fusion under Cooperative Agreement DE-FC03-92SF19460, the University of Rochester, and the New York State Energy Research and Development Authority. The support of DOE does not constitute an endorsement by DOE of the views expressed in this paper.

N. G. Usechak and G. P. Agrawal can be reached by e-mail at noodles@optics.rochester.edu and gpa@optics.rochester.edu, respectively.

REFERENCES AND NOTES

1. S. N. Vlasov, V. A. Petrishchev, and V. I. Talanov, "Averaged description of wave beams in linear and nonlinear media (the method of moments)," Radiophys. Quantum Electron. **14**, 1062–1070 (1971).
2. S. E. Harris and R. Targ, "FM oscillation of the He–Ne laser," Appl. Phys. Lett. **5**, 202–204 (1964).
3. G. Geister and R. Ulrich, "Neodymium-fiber laser with integrated-optic mode locker," Opt. Commun. **68**, 187–189 (1988).
4. D. J. Kuizenga and A. E. Siegman, "FM and AM mode locking of the homogeneous laser—Part I: Theory," IEEE J. Quantum Electron. **QE-6**, 694–708 (1970).
5. H. A. Haus and Y. Silberberg, "Laser mode locking with addition of nonliner index," IEEE J. Quantum Electron. **QE-22**, 325–331 (1986).
6. F. X. Kärtner, D. Kopf, and U. Keller, "Solitary-pulse stabilization and shortening in actively mode-locked lasers," J. Opt. Soc. Am. B **12**, 486–496 (1995).
7. J. G. Caputo, C. B. Clausen, M. P. Sørensen, and S. Bischoff, "Amplitude-modulated fiber-ring laser," J. Opt. Soc. Am. B **17**, 705–712 (2000).
8. H. A. Haus, D. J. Jones, E. P. Ippen, and W. S. Wong, "Theory of soliton stability in asynchronous modelocking," J. Lightwave Technol. **14**, 622–627 (1996).
9. N. G. Usechak, J. D. Zuegel, and G. P. Agrawal, "FM mode-locked fiber lasers operating in the autosoliton regime," IEEE J. Quantum Electron. **41**, 753–761 (2005).
10. K. Tamura and M. Nakazawa, "Pulse energy equalization in harmonically FM mode-locked lasers with slow gain," Opt. Lett. **21**, 1930–1932 (1996).
11. M. Nakazawa, H. Kubota, A. Sahara, and K. Tamura, "Time-domain *ABCD* matrix formalism for laser mode-locking and optical pulse transmission," IEEE J. Quantum Electron. **34**, 1075–1081 (1998).

12. A. M. Dunlop, W. J. Firth, and E. M. Wright, "Pulse shapes and stability in Kerr and active mode-locking (KAML)," Opt. Express **2**, 204–211 (1998).
13. S. Longhi and P. Laporta, "Time-domain analysis of frequency modulation laser oscillation," Appl. Phys. Lett. **73**, 720–722 (1998).
14. N. G. Usechak and G. P. Agrawal, "Semi-analytic technique for analyzing mode-locked lasers," Opt. Express **13**, 2075–2081 (2005).
15. D. J. Kuizenga and A. E. Siegman, "FM and AM mode locking of the homogeneous laser—Part II: Experimental results in a Nd:YAG laser with internal FM modulation," IEEE J. Quantum Electron. **QE-6**, 709–715 (1970).
16. M. Nakazawa, E. Yoshida, and K. Tamura, "10 GHz, 2 ps regeneratively and harmonically FM mode-locked erbium fibre ring laser," Electron. Lett. **32**, 1285–1287 (1996).
17. G. P. Agrawal, *Applications of Nonlinear Fiber Optics* (Academic, 2001).
18. N. R. Pereira and L. Stenflo, "Nonlinear Schrödinger equation including growth and damping," Phys. Fluids **20**, 1733–1734 (1977).
19. N. Akhmediev and A. Ankiewicz, eds., *Dissipative Solitons* (Springer, 2005).
20. E. Yoshida, K. Tamura, and M. Nakazawa, "Intracavity dispersion effects of a regeneratively and harmonically FM mode-locked erbium-doped fiber laser," IEICE Trans. Electron. **E81-C**, 189–194 (1998).
21. To remain consistent with Ref. 9, a Fabry–Perot laser cavity was simulated. In a Fabry–Perot cavity the light passes through each element twice during a single round trip; therefore, $\Delta_{FM} \rightarrow 2\Delta_{FM} = 0.9$ and $P_{sat} \rightarrow P_{sat}/2 = 12.5$ mW.
22. C. J. McKinstrie, "Effects of filtering on Gordon–Haus timing jitter in dispersion-managed systems," J. Opt. Soc. Am. B **19**, 1275–1285 (2002).
23. J. Santhanam and G. P. Agrawal, "Raman-induced spectral shifts in optical fibers: general theory based on the moment method," Opt. Commun. **222**, 413–420 (2003).
24. J. D. Kafka, T. Baer, and D. W. Hall, "Mode-locked erbium-doped fiber laser with soliton pulse shaping," Opt. Lett. **15**, 1269–1271 (1989).
25. T. Brabec, Ch. Spielmann, and F. Krausz, "Mode locking in solitary lasers," Opt. Lett. **16**, 1961–1963 (1991).
26. D. Kopf, F. X. Kärtner, K. J. Weingarten, and U. Keller, "Pulse shortening in a Nd:glass laser by gain reshaping and soliton formation," Opt. Lett. **19**, 2146–2148 (1994).
27. K. Tamura, E. Yoshida, and M. Nakazawa, "Forced phase modulation and self phase modulation effects in dispersion-tuned mode-locked fiber lasers," IEICE Trans. Electron. **E81-C**, 195–200 (1998).